

Generation of Depth Map for Future Free-view TV Using isotropic and anisotropic Complex diffusion de-noising using Depth Image Base Rendering (DIBR)

Farrukh Matloob^a, Kainat Arshad^b, Tariq Bashir^a

^aDepartment of Electrical and Computer Engineering, COMSATS University Islamabad, 45550, Islamabad, Pakistan

^bDepartment of Information Technology, University of the Punjab, Jhelum Campus, Pakistan

Submitted: 15-09-2021

Revised: 25-09-2021

Accepted: 28-09-2021

ABSTRACT: With the increased interest of users in 3D-TV system a number of techniques and methods have been developed to facilitate the users at home with 3D-TV. These techniques either rely on cumbersome techniques or required to have high bandwidth data transmission ability which lowers the feasibility of 3D-TV for common users. Further During the image acquisition process, a number of noises contaminated with the image pixels which reduce the image quality for further processing. A same problem occurs when a 3D view is generated from a 2D degraded image using DIBR. The occlusion effect occurs in the 3D view which lower its quality. In this research paper we presented a novel approach to de-noise the degraded 2D image using isotropic and anisotropic diffusion image de-noising and to generate the 3D view using DIBR for end users. The main purpose of the paper is to present a robust and novel technique which reduces the occlusion effect in the resultant 3D-view. Results of our novel approach have been tested on different available datasets in terms of PSNR, SSIM and UQI. Our results show that our approach performs better than the state of the art existing methods.

KEYWORDS: 3D-TV (3-Dimensional television), DIBR (Depth Image based rendering), isotropic and anisotropic diffusion, PSNR (Peak signal to noise

ratio), SSIM (structural similarity index metrics), UQI (Universal quality of image)

I. INTRODUCTION

In the early evolution of broadcasting people enjoyed the television in black and white. But with the passage of time people seemed more curious about watching 3D scene on their traditional television sets.

As the technology evolved technique of depth image based rendering developed to convert 2D image to 3D images. Use of depth image based rendering three dimensional television (DIBR-3DTV) technology changed the mode of entertainment of the end user. This new emerging technology has adopted by many entertainment entities like cinema, TV channels, and video games [1]. XBOX converted the 2D video games into 3D video games by using kinect camera [2]. So that people can enjoy games in more realistic way. Multiple media industries are gaining enormous benefits from DIBR-3D and their income increased exponentially e.g. 'Avatar'. This is released in 2009 and broke all the previous records of earning.

To achieve the good quality 3D-view at user end, a high quality depth map is basic requirement. Quality of the depth map produced by the algorithm heavily depends upon the quality of the input image. So, as we are using degraded image in our proposed system at

input, it is difficult to achieve the high quality depth map without proper image de-noising. Datasets we are using are corrupted with the Gaussian noise [3]. Here in our research paper we will use two image de-noising techniques namely isotropic complex diffusion and anisotropic complex diffusion. We will see that how they affect in reduction of occlusion effect in final 3D-View, and which technique will perform better. The concept of diffusion is taken from a physical process that equilibrates the quantitative difference. This equilibration property is expressed by Fick's law

$$j = -D \cdot \nabla u \quad (1)$$

In the above equation concentration gradient ∇u causes a flux j which aims to compensate for this gradient. The diffusion tensor D is an acting agent between ∇u and j . The case in which j and ∇u are parallel called isotropic diffusion and the case where j and ∇u are not parallel called anisotropic diffusion. It is observed that diffusion only transport mass from one place to another without destroying or creating it. Hence this diffusivity can be represented with the help of equation of continuity as given below

$$\partial_t u = -\text{div } j \quad (2)$$

Where t denotes the time. If we combine the Fick's law with equation of continuity then diffusion equation becomes as below

$$\partial_t u = \text{div } (D \cdot \nabla u) \quad (3)$$

In image processing we may define the concentration as the grey value at certain block of the image. If the diffusion tensor is constant over the whole image, then it is called homogeneous diffusion, and if it is the space-dependent then it is called inhomogeneous diffusion. In computer vision literature homogeneous diffusion is termed as isotropic and inhomogeneous diffusion as anisotropic diffusion. After image de-noising in our proposed system next step is depth map generation. To generate a high quality 3D view using DIBR (Depth image based rendering) a high quality depth map is a basic need, so that every object in final 3D scene could be viewed clearly. The existing

methods uses pristine images to find depth map using stereo matching algorithms and apply post processing methods to remove the occlusion. These post processing methods include hole filling, confident matching and application of weighted median filter etc. This post processing takes much time to produce the fine results, hence the efficiency of the overall algorithm is slows down [4].

In this research work, we presented an efficient method which takes a noisy/degraded image. In the first part of our algorithm we will de-noise the image using isotropic complex diffusion technique or anisotropic complex diffusion technique and in the second part depth map from de-noised single image is estimated. Central to this second part, the use of phase shift theorem in Fourier domain to produce a sub aperture image. This sub-aperture image will slightly differ from the de-noised image in terms of baseline distance. In other words we have a shorter baseline distance between the de-noised and sub-aperture image. Further this sub-aperture image is used for stereo correspondence. Then cost volume is computed to find matching cost which is further used for similarity measurement. Gradient matching costs are also evaluated based on the angular coordinates of the camera. After estimation of the depth map, the input image and this produced depth map will be used to produce the left and right virtual views using the process of DIBR. Then moving on the process further the anaglyph image is produced. The hole percentage produced in generating the left and right virtual views shows the occlusion effect produced in the image. This paper aims to produce the lowest occlusion effect in terms of hole percentage than the previously published state of the art techniques.

The effectiveness of the algorithm is tested on the dataset [3]. A performance comparison is also presented with [32] and [33].

The rest of the paper is organized as follows: In section 2, literature review is explained. Section 3 presents proposed methodology. Section 4 explains Experimental results and discussion. Section 5 shows conclusion and finally section 6 lists the bibliography.

Literature review

Generation of 3D-view using depth image based rendering is a new evolving technology in the field of television entertainment. To generate a high quality 3D-view a high quality depth map is needed, and to generate depth map of good quality the input image to the depth map estimation algorithm must noise free as much as possible. A pristine image will generate the good quality depth map. Focusing on the need of image de-noising in the process of DIBR a lot of work has been published to de-noise the images. Conventional image de-noising methods such as 2D Gaussian filter, median filter are efficient in de-noising, but the problem is they blur the image edges. So there is a need to find out the new ways to de-noise the images so that image details preserved. Tudor Barbu [5] implemented an improved version of Perona-Malick non-linear diffusion model. Their model contains a novel diffusivity function and they explained mathematical reason, that how, his model is improved version of the Perona-Malick non-linear diffusion model and justified. So their proposed PDE- based smoothing technique provided the state of the art results. V.B. Surya Prasath [6] realized that images contain multiple scales objects and the homogeneous noise removal algorithm removes the noise disrupting all edges details so they proposed a multi-scale anisotropic image de-noising technique. Their proposed scheme gathers the inter scale information and provides excellent noise removal and edges preservation. Feng liu et al [7] proposed a diffusion tensor which adaptively determines the intensities of the image in four directions to determine the structure of the image. This diffusion acted as isotropic in the interior region of the image and as anisotropic at the edges. Mrazek et al [8] studied the relation between diffusivity and shrinkage of the Haar wavelet and showed that both the methods are equivalent.

The next step to image de-noising is to find the depth map. Literature survey related to depth map shows that depth map estimation could be divided into two categories i.e. automatic and semi-automatic. In automatic methods depth cues are estimated in the image then these depth cues are translated as the foreground and background [9], [10]. Yang et al.[11]

presented an approach which categorizes an image into three sections. Then depth map of every section is produced. Huang et al.[12]estimated defocus or blur details of the image then using wavelet transformation and canny edge detector estimated the depth map. A method to estimate the depth of moving objects is presented in [13]. Tsai et al [14]presented a Gaussian mixture model and super pixel linear iterative clustering algorithm to produce the depth map. After this, they refined the depth map by acquiring edges information and by using various path modes. Estimation of depth map by calculating the sum of absolute difference SAD of two adjacent pixels of two same images is represented in[15]. William et al. [16] proposed an approach to estimate depth map from its anaglyph version. Philippe Leclercq and John Morris uses Census transform algorithm with image segmentation to compute matching costs in the presence of noise and showed that performance of the area based matching cost decreases as the signal to noise ratio (SNR) decreases below 36dB [17]. Olga Krutikova et al explained how to reconstruct 3D model of face by finding accurate depth map. They placed a mask on the image which uses a sliding window in the pre-processing to rectify the image [18]. Aamir Saeed Malik and Tae-Sun Choi proposed a new image focus method to find the depth map and proved the drastic improvement in results if the input images contains different noises [19]. Yong Seok Heo et al proposed a new method that find stereo matching costs between two images and de-noise the input images simultaneously. They used NL-means algorithm for restoration of pixels intensity values and perceptually modified Housdorff distance (PMHD) for the calculation of dissimilarity of supporting pixels distribution [20]. Viral H. Borisagar et al image based segmentation and census transform to find the depth map and showed that it works better in noisy environment [21]. Further there are some common methods to estimate the depth map from clean image like Nagai et al proposed a technique for surface reproduction from a solitary picture for known fixed objects such as hands, face etc. [22]. Hertzmann et al reconstructed a 3-D model for several images but they required that an assistant object whose shape is known is present next to the target object [23]. Torralba and Oliva discussed Fourier spectrum of the images to find

the depth of image [24]. Michel, Saxena and Ng used supervised learning of 1-D distances of objects [25].

Semi-automatic techniques also have been developed to generate the depth map. Generation of depth map using local depth hypothesis. The dark color is assigned to the objects which belong to the vanishing point in the image and the bright color is assigned to the objects which belong to the foreground in the image [26]. Phan et al. [27] presented the scale space random walk and graph cut segmentation to generate the depth map. All the above explained techniques of depth map generation are the efforts to estimate the more accurate depth map so that scene interpretation which is required in the most of the real world application could be done more accurately.

However the conventional systems are performing better in generating the 3D-view but the problem is they require a high bandwidth to transmit the much cumbersome information to receiver end to generate the 3D scene. This also required system training and cumbersome research to find out the corresponding results. To transmit the 3D-TV data efficiently, then transmission of the data and information requires compression and due to this compression data get corrupted and the occlusion effect is produced [28]. Degraded dataset is de-noised and using discrete cosine transform DCT by considering the three attributes i.e. brightness, contrast and color [29]. Yang et al [30] presented multi-lateral guided filter to enhance the degraded depth map. In our proposed system noisy (Gaussian noise) images are enhanced/ de-noised using isotropic and anisotropic diffusion techniques separately. Then depth map from this de-noised image is estimated. Following the depth map estimation, the original input image and estimated depth map are fed to DIBR process to generate the right virtual view and left virtual view, and hole percentage is calculated to estimate the occlusion effect. Then these left and right virtual views are used to generate the anaglyph image. The tested dataset is available online [3] and it is used with term of service for the website.

II. Enhancement of depth map using depth image based rendering (EDDIBR)

An efficient and detailed proposed methodology is illustrated in the figure 1. This proposed scheme consists of two main steps to generate a 3D view from degraded 2D image. In the first step image de-noising using isotropic or anisotropic complex diffusion is performed. Working of both the algorithms is different, isotropic complex diffusion works better when the noise is evenly distributed and anisotropic complex diffusion works well when the diffusion of noise in the image is not evenly distributed. Next to the image de-noising is to estimate the depth map from this de-noised version. Accuracy of the per pixel's depth information lies in the quality of the de-noised image. A high quality de-noised image will produce a good quality depth map and eventually the occlusion effect will be reduced in the 3D image. After that this depth map and input image is fed to DIBR process to generate the right and left virtual views. Then these right and left images are used to generate an anaglyph image.

Isotropic complex diffusion

Isotropic complex diffusion could be represented as

$$\partial_t u = \nabla u \quad (4)$$

$$u(x, 0) = f(x) \quad (5)$$

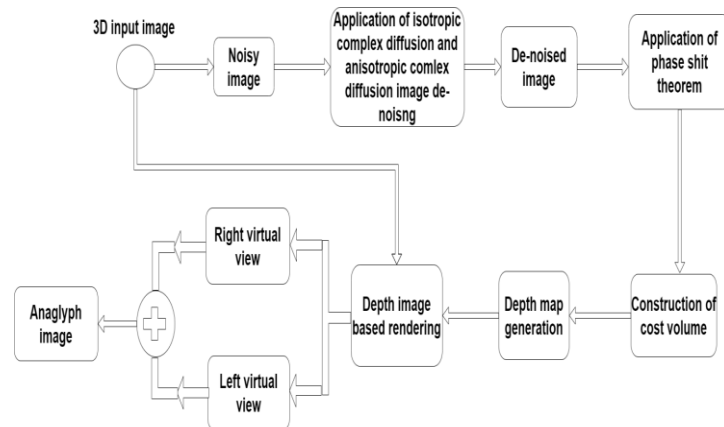


Figure 1. Proposed Methodology

These equation possess the solution as below

$$u(x, t) = \begin{cases} f(x) & (t = 0) \\ (K_{\sqrt{2T}} * f)(x) & (t > 0) \end{cases} \quad (6)$$

The solution represented in the above equation is unique, provided that it satisfies with conditions mentioned.

$$|u(x, t)| \leq M \cdot \exp(a|x|^2) \quad (M, a > 0) \quad (7)$$

It depends continuously on the initial image f with respect to $\|\cdot\|_{L^\infty \mathbb{R}^2}$, and it fulfills the maximum-minimum principle.

$$\inf f \leq u(x, t) \leq \sup f \quad \text{on } \mathbb{R}^2 \times [0, \infty) \quad (8)$$

From equation it could be observed that the time t is related to the spatial width σ requires stopping the diffusion process at time

$$T = \frac{1}{2} \sigma^2 \quad (9)$$

Anisotropic complex diffusion

Perona and Malick proposed anisotropic complex diffusion method to de-noise the image and to remove the localization problem of linear diffusion. They applied an inhomogeneous function that eliminates the diffusivity at the locations in the image which have greater similarity to be edges. This similarity or likelihood is aggregated by $|\nabla u|^2$. The Perona-Malick anisotropic diffusion function is based on the following equation.

$$\partial_t u = \text{div} (g(|\nabla u|^2) \nabla u) \quad (10)$$

Above equation uses diffusivity such as

$$g(s^2) = \frac{1}{1 + \lambda^2 s^2} \quad (\lambda > 0) \quad (11)$$

Equation [10] and [11] represents the full structure of the complex anisotropic diffusion. To observe the effect of improved anisotropic complex diffusion at edges let

us refrain ourselves to the one-dimensional case. This scenario simplifies the notations and main working since near a straight edge a two dimensional function changes to a function of one variable. For the purpose of diffusivity, it follows that the flux function $\phi(s) = sg(s^2)$ satisfies $\phi'(s) \geq 0$ for $|s| \leq \lambda$, and $\phi'(s) < 0$ for $|s| > \lambda$, so equation 10 can be rewritten as

$$\partial_t u = \Phi'(u_x) u_{xx} \quad (12)$$

It could be observed that function in equation 12 is forward parabolic type for $|u_x| \leq \lambda$, and backward parabolic function for $|u_x| > \lambda$. Here in the eq. 12 λ plays the role of a contrast parameter separating forward from backward diffusion areas. It is easy to verify that improved complex anisotropic diffusion increases the slope at inflection points of edges within the backward area. Then there exist a smooth solution u which satisfies

$$\partial_t (u_x^2) = 2u_x \partial_x (u_t) = 2\Phi''(u_x) u_x u_{xx}^2 + 2\Phi'(u_x) u_x u_{xxx} \quad (13)$$

The point x_0 where u_x^2 is maximum at time t is characterized as $u_x u_{xxx} = 0$ and $u_x u_{xxx} \leq 0$. So

$$(\partial_t (u_x^2))(x_0, t) \geq 0 \quad \text{For } |u_x(x_0, t)| > \lambda \quad (14)$$

With strict inequality for $u_x u_{xxx} < 0$. For two dimensional cases above equation becomes as

$$\partial_t u = \Phi'(\nabla u) u_{\eta\eta} + g(|\nabla u|^2) u \quad (15)$$

Where ξ denotes the gauge coordinates and η depicts the perpendicular and parallel directions to ∇u . So, now we have forward diffusion along isophotes combined with forward and backward diffusion along flow lines. It could also be observed that forward-backward is not restricted to spatial diffusivity but it appearing in all diffusivities.

Depth map estimation

In preprocessing we have de noised our input image. In order to estimate the depth map from single de noised

image we are needed to create its sub aperture image which is created by using the Eq 16. of phase shift theorem in 2D Fourier transform. So by using phase shift theorem we created a sub aperture image so that we could utilize it for finding two complementary costs: namely sum of Absolute difference (SAD) and Sum of gradient difference (GRAD). Cost volume for these two

$$f(x + \Delta x) = f\{I(x)\} \exp(2\pi i \Delta x) \quad (16)$$

costs is given by Eq 17.

$$C(x, l) = \alpha C_A(x, l) + (1-\alpha) C_G(x, l) \quad (17)$$

Where cost volume is the function of x and l is the cost label and $\alpha \in [0,1]$, it is used to adjust the relative importance of the two complementary costs. Sum of absolute difference cost (C_A) is defined as

$$C_A(x, l) = \sum_{S \in v} \sum_{x \in R_x} \min(|I(S_c, x) - I(s, x) + \Delta x(s, l)|, \tau_1) \quad (18)$$

Where R_x is a small rectangular window function which is centered at the pixel, τ_1 is a threshold value to select a minimum cost volume and v contains the two Cartesian coordinates of the input image. The second complementary cost which is gradient cost (C_G) is defined as

$$C_G(x, l) = \sum_{S \in v} \sum_{x \in R_x} \beta(s) \min(Diff_x(S_c, S, X, l), \tau_2) + (1 - \beta(s)) \min(Diff_y(S_c, S, X, l), \tau_2) \quad (19)$$

Where $Diff_x(S_c, S, X, l) = |I_x(S_c, X) - I_x(S, X + \Delta X(S, l))|$ depicts the gradient cost in the x axis. Where as $Diff_y$ is the gradient cost in the y axis of sub aperture image. τ_2 is the minimum threshold value for the gradient cost. $\beta(s)$ navigates the relative importance of the two directional gradient cost. These two costs are further used to estimate the depth map of the de noised image[31].

Depth Image based Rendering

Depth image based rendering (DIBR) is a method to generate a synthesized virtual view in 3D. It is obtained by combining the reference input image and the depth map. Basically DIBR is based on two synthesized image namely left and right virtual images which are obtained by 3D warping equations 20 and 21.

$$(X_r, Y) = X_c - \frac{t_x}{2} * \frac{f}{d} \quad (20)$$

$$(X_l, Y) = X_c + \frac{t_x}{2} * \frac{f}{d} \quad (21)$$

Where (X_r) and (X_l) are right and left image pixel position, X_c is the center of the image, t_x is the baseline or distances of the two lenses of the camera, f is the focal length of the camera and d is the depth map of the corresponding image. During this process occlusion might occur when input image is synthesized to left and right virtual images.

III. Results and Discussion

In this section implementation details and comparison of our proposed algorithms with previously published

state of the art techniques is presented in detail. To compare the performance of proposed system commonly used performance matrices are used such as PSNR, SSIM, UQI and the hole percentage to show the reduced occlusion effect. Visual performance of our both proposed techniques of converting a degraded 2D image to 3D-view i.e. using isotropic complex diffusion and anisotropic complex diffusion is also presented in this section. Following the visual performance we presented the quantitative performance of the proposed system in terms of PSNR, SSIM and UQI is presented. After that hole percentage comparison is given to show the superiority of the proposed techniques. To further show the better performance of the proposed system we evaluated our 3D results in detail. For this purpose we presented the PSNR comparison of left and right virtual views generated by our proposed techniques both with left and right view generated using noisy depth map and with state of the art techniques. All evaluation techniques show that our proposed techniques perform

better than previously published state of the art techniques.

Implementation Details

The proposed system is implemented in MATLAB 2017Ra on Dell core i5 having 2.4 GHz processor, 6GB RAM. It takes around 90 seconds to execute the algorithm. For results validation and comparison with other state of the art techniques datasets from [3] is used. Size of data sets used is 512×512 . All the images are degraded with Gaussian noise. To check and verify

the results of the conversion of degraded 2D image to 3D view noise variance of the 0.06 is introduced in the dataset [3].

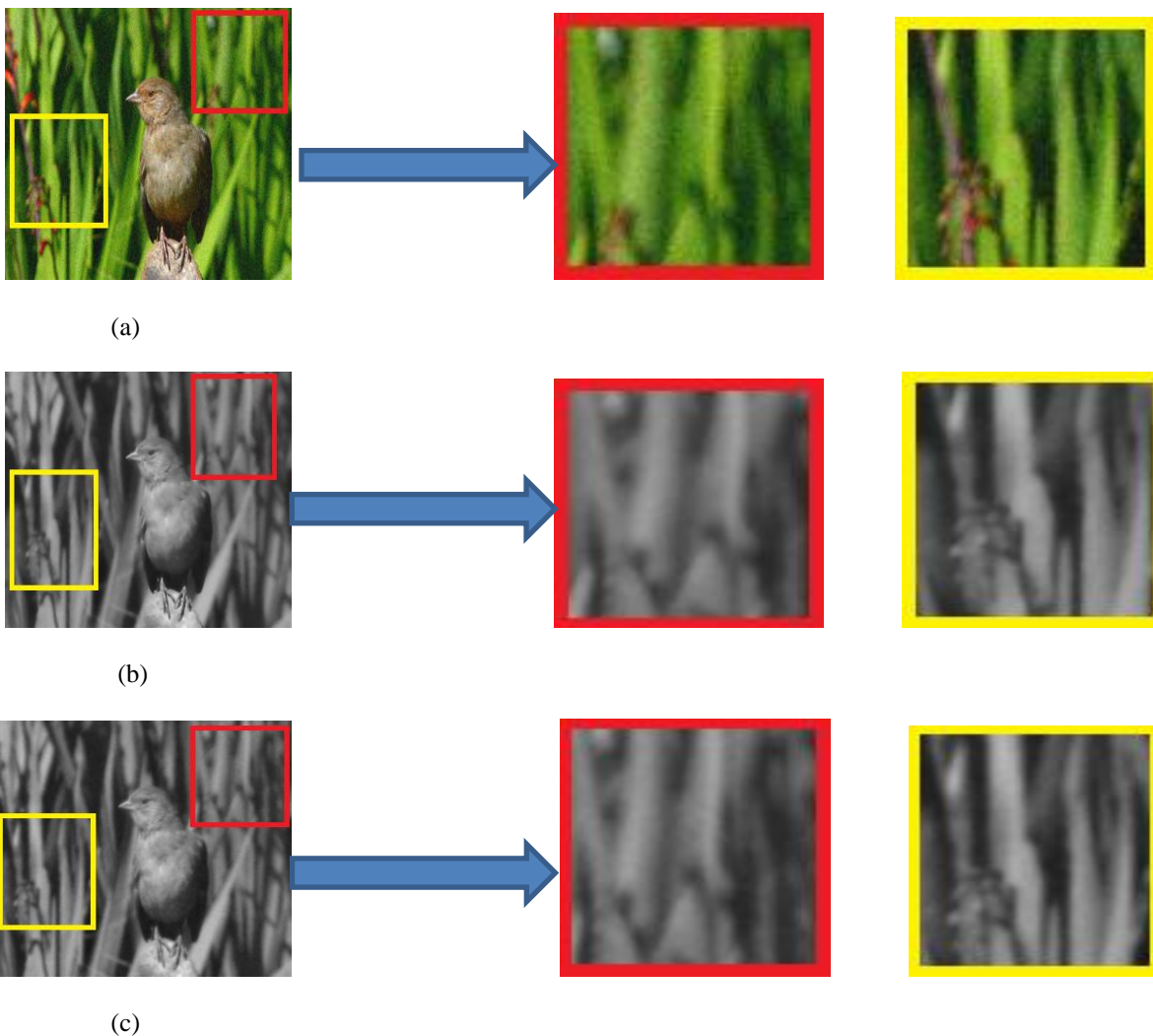


Fig.2 (a) Noisy Image (b) De-noised image using Isotropic complex diffusion (c) De-noised image using anisotropic Complex diffusion

Image de-noising performance

Image de-noising is the key point in our proposed system as it lowers the occlusion effect in the resultant 3D image. Figure 3 and figure 4 show the performance of isotropic complex diffusion and anisotropic complex diffusion image de-noising respectively. From visual performance of these two figures it could be concluded that anisotropic complex diffusion performs better than the first one. Moreover it could also be noted that both the techniques de-noised the images with very minute

difference and smooth the pixels intensity level. Due to which images appeared to be slightly blur. This phenomenon could also be observed from the figure 2 figure 3 and figure 4, where pixels intensity level is reduced after application of both the de-noising techniques. But slight reduction in intensity level does not disrupt the edges of the image and image structure purely belongs to its original counterpart. Figure 3 and figure 4 verifies the phenomenon that after de-noising image structure exactly co-relates with its original one.

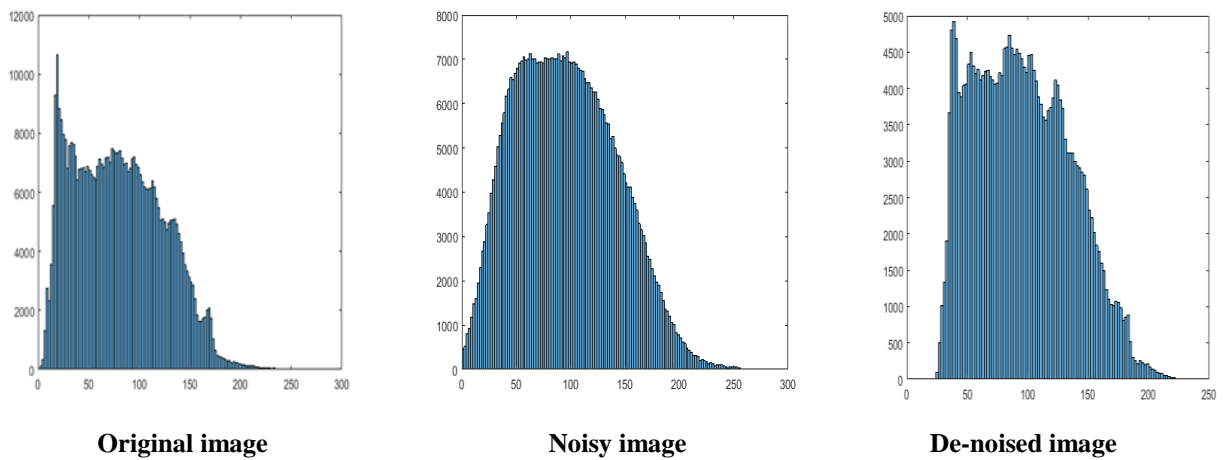


Figure 3. Image de-noising performance using isotropic complex diffusion in histogram

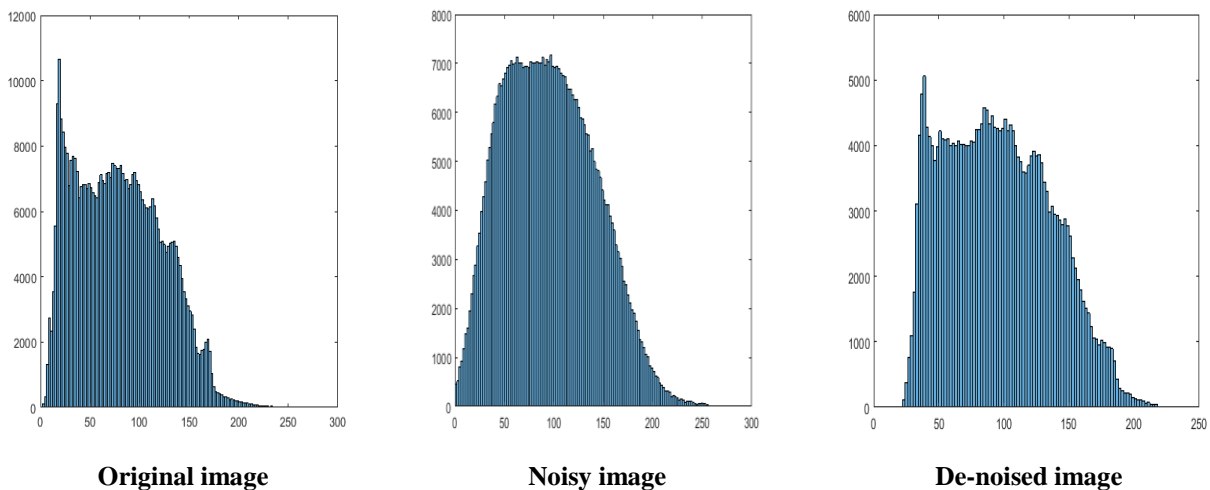


Fig.4 Image de-noising performance using anisotropic complex diffusion in histogram

Visual performance of proposed system using 3D-DIBR

Primary task of this research paper is to introduce a technique which is an efficient and offers lowest occlusion effect at the receiver side using 3D-DIBR. So a visual performance of the proposed system using both the techniques i.e. using isotropic complex diffusion and anisotropic complex diffusion is shown in the figure 5 and figure 6 respectively. It could be noticed from figure 5 and figure 6 that visual performance of the proposed system using anisotropic system is much better than the

performance of the proposed isotropic system. The left and right virtual views generated by proposed anisotropic approach are more clear and crisp than the left and right virtual views generated by the proposed isotropic complex diffusion technique. From figure 5 and figure 6 it could also be concluded that the anaglyph image generated by the anisotropic complex diffusion technique is more refined and crisp than the generated by proposed isotropic complex diffusion technique.

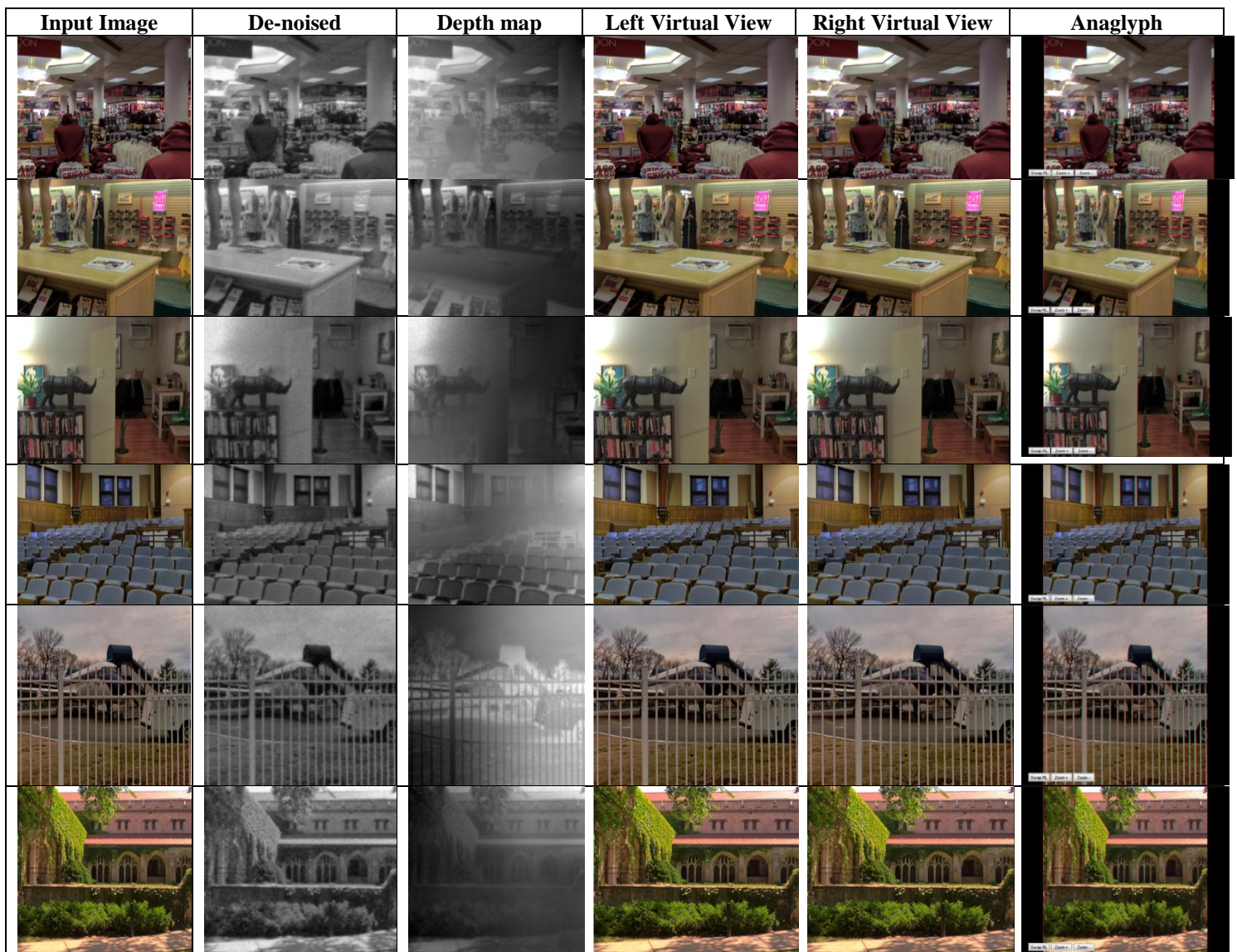


Fig.5 Proposed system performance using isotropic complex diffusion image de-noising




































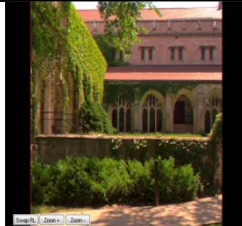
Input Image	De-noised	Depth map	Left Virtual View	Right Virtual View	Anaglyph
					
					
					
					
					
					

Fig.6 Proposed system performance using anisotropic complex diffusion image de-noising

Image No.	Zhuo et al			IU Afridi et al			Proposed Isotropic Complex Diffusion			Proposed anisotropic Complex Diffusion		
	PSNR	SSIM	UQI	PSNR	SSIM	UQI	PSNR	SSIM	UQI	PSNR	SSIM	UQI
1	13.2008	0.3057	0.735	6.7711	0.313	0.5127	13.7049	0.5062	0.7594	14.0537	0.5338	0.7481
2	13.0968	0.3645	0.7871	7.995	0.3568	0.6412	15.254	0.5687	0.8511	13.1123	0.471	0.6931
3	8.4694	0.284	0.5862	7.461	0.4895	0.5435	13.8022	0.4003	0.7003	16.09	0.5566	0.7209
4	12.7106	0.2414	0.7603	7.4501	0.4232	0.5354	15.9934	0.4797	0.8434	13.9889	0.4688	0.7838
5	14.5583	0.4009	0.8252	8.7812	0.3814	0.6517	11.9091	0.2384	0.7806	10.0235	0.2008	0.6659
6	14.2722	0.3576	0.7895	8.1837	0.2624	0.5712	15.8983	0.4598	0.8158	14.7498	0.437	0.7597

Table 1. PSNR ,SSIM and UQI comparison with [32] and [33]

Quantitative performance of proposed system using 3D-DIBR

The basic requirement to produce the high quality 3D image for 3D-TV is to generate a high quality depth map. Here in the table 1 we presented the PSNR, SSIM and UQI comparison (in dB) of the proposed system with [32] and [33]. From table 1 it is clear that our proposed system performs better in terms of PSNR, SSIM and UQI of the depth map, by both techniques i.e proposed isotropic and anisotropic complex diffusion. Bold entries show the higher value in the table. Better PSNR depicts that obtained depth map has high quality in terms of edges clarity and objects detection present in the image.

Mean absolute error Comparison (MAE)

To estimate the error between the depth map and its ground truth Mean absolute error (MAE) is presented in the fig 7. Higher values of the MAE depict the greater degradation of the depth map during its generation resulting a greater pixels intensity difference between the depth map and its ground truth. On the other hand lower values of the MAE reflect the lower pixel's intensity difference resulting in better quality of the depth map.

From fig.8 it could be observed that our proposed techniques namely isotropic complex diffusion and anisotropic complex diffusion performed better than the

state of the art previously published techniques. So quality of the depth maps generated with proposed techniques have superior quality in terms of the MAE than the [32] and [33].

Root mean square error comparison (RMSE)

Root mean square error performance and its comparison

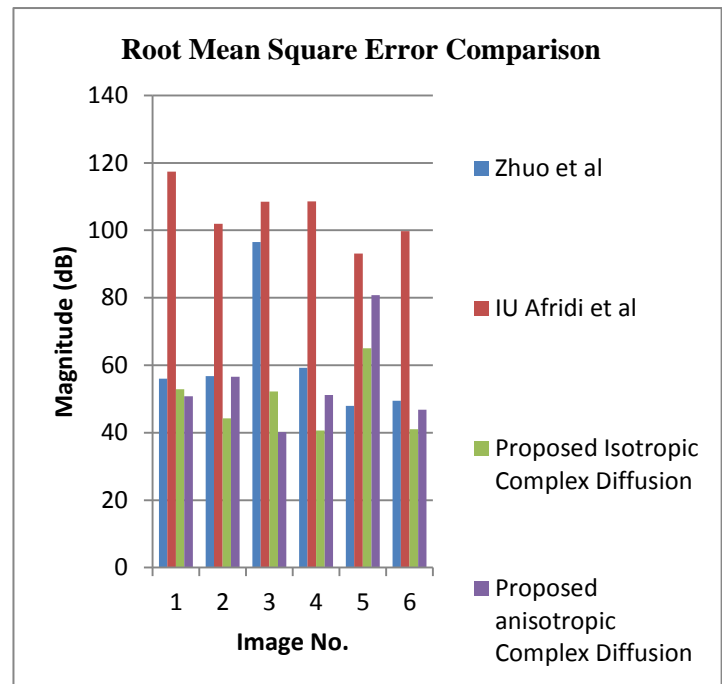


Fig.8 RMSE (in dB) comparison with [32] and [33].

with [32] and [33] is presented in the fig 8. From fig 9 it could be observed that our both proposed techniques much better than the previously published state of the art techniques [32] and [33]. It could also be observed that anisotropic complex diffusion technique performed better than the proposed isotropic complex diffusion technique. Values of RMSE obtained using proposed anisotropic complex diffusion are much lower (which is better), so visual quality of the depth map using this technique more is better than the depth maps obtained Using proposed isotropic complex diffusion.

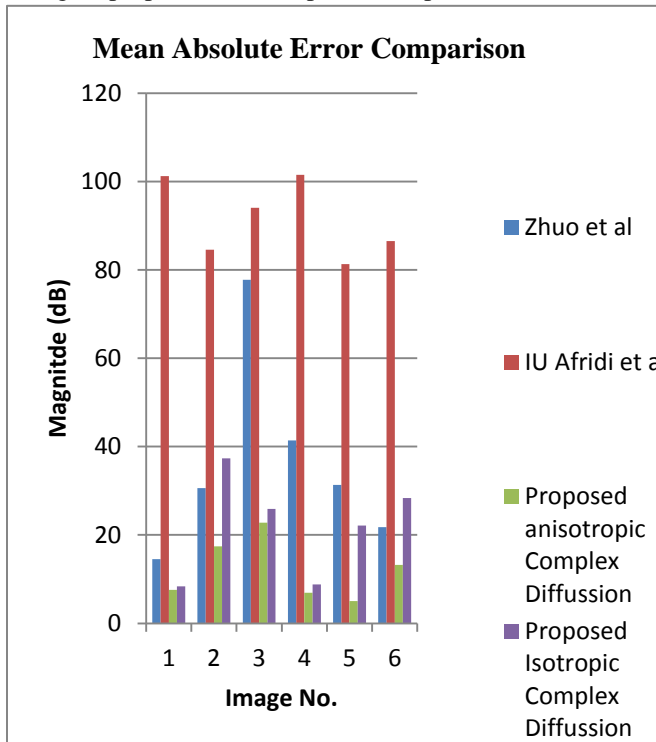


Fig.7 MEA comparison (in dB) with [32] and [33]

Hole percentage Comparison

Hole percentage comparison of the proposed techniques with previously published state of the art techniques [32] and [33] is presented in the table 2. Percentages of holes found in creation of the left and right virtual views are actual measurement of occlusion produced in the process of DIBR. A comparison of hole percentages with the state of the art previously published techniques is presented in the table 2. Bold values in the table shows the lowest hole percentage for the respective image. From table 2 we could conclude that both of our presented techniques to generate 3D-view from a 2D degraded image has outperformed than the previously published techniques. The lowest value of the hole percentage shows the higher quality of the left and right virtual views produced. Hence the quality of the anaglyph image produced by using these left and right virtual image will be up to mark. From the table 2 we could conclude that on averagely our proposed anisotropic complex diffusion technique performed better than the proposed isotropic complex diffusion technique. Table 2 shows that difference of the hole percentages of the proposed isotropic complex diffusion and proposed anisotropic complex diffusion techniques is approximately 0.001 or 0.0001, which is very minute difference. That's why the results produced by both the techniques are much better than the previously published techniques.

Image No	Zhuo et al		IU Afridi et al		Proposed isotropic Complex diffusion		Proposed anisotropic Complex diffusion	
	Left	Right	Left	Right	Left	Right	Left	Right
1	0.0155	0.0156	0.0053	0.0053	0.003	0.003	0.0044	0.0024
2	0.0132	0.0132	0.0052	0.0052	0.0023	0.0023	0.0021	0.0021
3	0.0507	0.0505	0.0048	0.0048	0.0044	0.0044	0.003	0.0033
4	0.0165	0.0165	0.0055	0.0055	0.0026	0.0026	0.0028	0.0027
5	0.0158	0.0158	0.0055	0.0055	0.003	0.003	0.0027	0.0027
6	0.0044	0.0044	0.0053	0.0053	0.0028	0.0028	0.0024	0.0024

Table.2 Holes percentages comparison with [32] and [33]

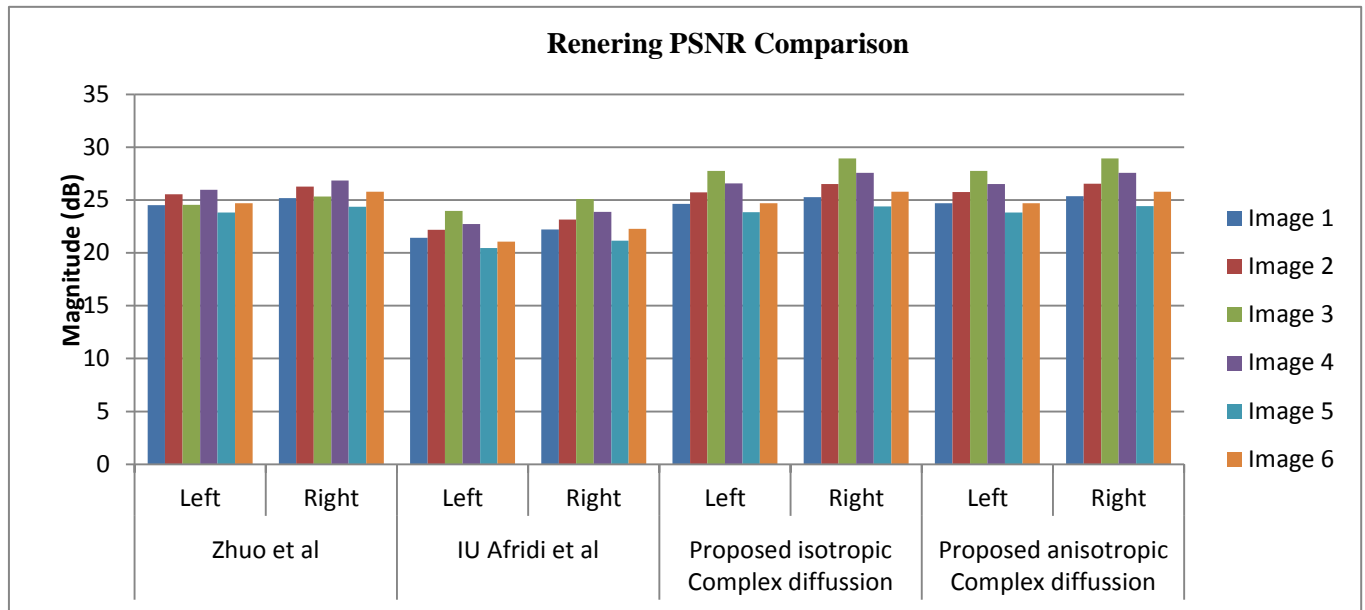


Fig.9 Rendering PSNR comparison with [32] and [33]

Rendering Performance of proposed algorithms

To show the overall performance of DIBR of proposed technique, PSNR comparison between depth image based rendering of [32] and [33] and depth image based rendering of the proposed techniques is presented in the fig 9. It could be seen that PSNR values of the left and right virtual views generated by using the proposed techniques are much better than the PSNR values of the left and right virtual views generated by the [32] and [33]. This performance shows that image de-noising techniques performed well on noisy images and played a major role to reduce the occlusion effect in the left and right virtual views. Improved PSNR value of the Left and right virtual views also reflects the better performance of the depth map generation and rendering algorithms. So from fig.9 it is clearly observed that both the proposed techniques performed better than the state of the art previously published techniques [32] and [33]. From fig10 we further could observe that proposed anisotropic complex diffusion technique performed slightly better than the proposed isotropic complex diffusion.

IV. Conclusions

In this research paper two novel approaches are presented to generate high quality 3D view for 3D-TV from degraded 2D image using depth image based rendering (DIBR). Two image de-noising techniques are presented namely isotropic complex diffusion and anisotropic complex diffusion. Figure 6 and figure 7 shows the visual performance superiority of the proposed techniques. From quantitative analysis presented in the table 1 to table 6 it is concluded that our proposed techniques performed much better than the state of the art techniques [32], [33]. It is also observed from table 1 to table 6 that anisotropic complex diffusion image de-noising offers best performance to reduce the occlusion effect in the resultant 3D-view. Hence the quality of the 3D-view generated using DIBR is increased.

V. References

- [1] Z. Zhang, "Microsoft Kinect Sensor and Its Effect," *IEEE Multimed.*, vol. 19, no. 2, pp. 4–10, Feb. 2012.
- [2] J. Andrews and N. Baker, "XBOX 360 SYSTEM ARCHITECTURE," *IEEE MICRO*, p. 13, 2006.
- [3] C. Rhemann, C. Rother, J. Wang, M. Gelautz, P. Kohli, and P. Rott, "A Perceptually Motivated Online Benchmark for Image Matting," p. 8.
- [4] H.-G. Jeon *et al.*, "Accurate depth map estimation from a lenslet light field camera," in *2015 IEEE Conference on Computer Vision and Pattern Recognition (CVPR)*, Boston, MA, USA, 2015, pp. 1547–1555.
- [5] T. Barbu, "Robust Anisotropic Diffusion Scheme for Image Noise Removal," *Procedia Comput. Sci.*, vol. 35, pp. 522–530, 2014.
- [6] V. B. S. Prasath, "Image denoising by anisotropic diffusion with inter-scale information fusion," *Pattern Recognit. Image Anal.*, vol. 27, no. 4, pp. 748–753, Oct. 2017.
- [7] F. Liu and J. Liu, "Anisotropic diffusion for image denoising based on diffusion tensors," *J. Vis. Commun. Image Represent.*, vol. 23, no. 3, pp. 516–521, Apr. 2012.
- [8] P. Mrázek, J. Weickert, and G. Steidl, "Correspondences between Wavelet Shrinkage and Nonlinear Diffusion," in *Scale Space Methods in Computer Vision*, vol. 2695, L. D. Griffin and M. Lillholm, Eds. Berlin, Heidelberg: Springer Berlin Heidelberg, 2003, pp. 101–116.
- [9] Y. Xiong and S. A. Shafer, "Depth from focusing and defocusing," in *Proceedings of IEEE Conference on Computer Vision and Pattern Recognition*, New York, NY, USA, 1993, pp. 68–73.
- [10] A. S. Malik, S.-O. Shim, and T.-S. Choi, "Depth Map Estimation using a Robust Focus Measure," in *2007 IEEE International Conference on Image Processing*, San Antonio, TX, USA, 2007, pp. VI-564-VI-567.
- [11] Y. Yang, X. Hu, N. Wu, P. Wang, D. Xu, and S. Rong, "A Depth Map Generation Algorithm Based on Saliency Detection for 2D to 3D Conversion," *3D Res.*, vol. 8, no. 3, p. 29, Sep. 2017.
- [12] D.-F. Huang, Y.-H. Chen, and T.-W. Huang, "Using Wavelet Transformation and Edge Detection to Generate a Depth Map from a Single Image," *Smart Sci.*, vol. 5, no. 2, pp. 75–84, Apr. 2017.
- [13] C. Jung, L. Wang, X. Zhu, and L. Jiao, "2D to 3D conversion with motion-type adaptive depth estimation," *Multimed. Syst.*, vol. 21, no. 5, pp. 451–464, Oct. 2015.
- [14] T.-H. Tsai, T.-W. Huang, and R.-Z. Wang, "A novel method for 2D-to-3D video conversion based on boundary information," *EURASIP J. Image Video Process.*, vol. 2018, no. 1, p. 2, Dec. 2018.
- [15] L. Bolecek and V. Rícný, "The estimation of a depth map using spatial continuity and edges," in *2013 36th International Conference on Telecommunications and Signal Processing (TSP)*, Rome, Italy, 2013, pp. 890–894.
- [16] Williem, R. Raskar, and I. K. Park, "Depth Map Estimation and Colorization of Anaglyph Images Using Local Color Prior and Reverse Intensity Distribution," in *2015 IEEE International Conference on Computer Vision (ICCV)*, Santiago, Chile, 2015, pp. 3460–3468.
- [17] P. Leclercq and J. Morris, "Robustness to noise of stereo matching," in *12th International Conference on Image Analysis and Processing, 2003.Proceedings.*, Mantova, Italy, 2003, pp. 606–611.
- [18] O. Krutikova, A. Sisojevs, and M. Kovalovs, "Creation of a Depth Map from Stereo Images of Faces for 3D Model Reconstruction," *Procedia Comput. Sci.*, vol. 104, pp. 452–459, 2017.
- [19] A. S. Malik and T.-S. Choi, "A novel algorithm for estimation of depth map using image focus for 3D shape recovery in the presence of noise," *Pattern Recognit.*, vol. 41, no. 7, pp. 2200–2225, Jul. 2008.
- [20] Y. S. Heo, K. M. Lee, and S. U. Lee, "Simultaneous Depth Reconstruction and Restoration of Noisy Stereo Images using Non-local Pixel Distribution," in *2007 IEEE Conference on Computer Vision and Pattern Recognition*, Minneapolis, MN, USA, 2007, pp. 1–8.
- [21] V. H. Borisagar and M. A. Zaveri, "Disparity Map Generation from Illumination Variant Stereo Images Using Efficient Hierarchical Dynamic Programming," *Sci. World J.*, vol. 2014, pp. 1–12, 2014.
- [22] T. Nagai, M. Ikehara, and A. Kurematsu, "HMM-based surface reconstruction from single images," *Syst. Comput. Jpn.*, vol. 38, no. 11, pp. 80–89, Oct. 2007.

- [23] A. Hertzmann and S. M. Seitz, "Example-based photometric stereo: shape reconstruction with general, varying BRDFs," *IEEE Trans. Pattern Anal. Mach. Intell.*, vol. 27, no. 8, pp. 1254–1264, Aug. 2005.
- [24] "A. Torralba and A. Oliva. Depth estimation from image structure - Google Search." [Online]. Available: https://www.google.com/search?source=hp&ei=W119XMi7FMGKmwWuzYmIBg&q=A.+Torralba+and+A.+Oliva.+Depth+estimation+from+image+structure&btnK=Google+Search&oq=A.+Torralba+and+A.+Oliva.+Depth+estimation+from+image+structure&gs_l=psy-ab.3...2344.2344..3508...0.0..0.536.536.5-1.....0....2j1..gws-wiz.....0.ey0D-KoHVeI. [Accessed: 04-Mar-2019].
- [25] "J. Michels, A. Saxena, and A.Y. Ng. High speed obstacle avoidance using monocular vision and reinforcement learning - Google Search." [Online]. Available: https://www.google.com/search?ei=X119XOmOMtGdkgX1mIKwDw&q=J.+Michels%2C+A.+Saxena%2C+and+A.Y.+Ng.+High+speed+obstacle+avoidance+using+monocular+vision+and+reinforcement+learning&oq=J.+Michels%2C+A.+Saxena%2C+and+A.Y.+Ng.+High+speed+obstacle+avoidance+using+monocular+vision+and+reinforcement+learning&gs_l=psy-ab.12...131706.138731..140721...0.0..0.0.0....5....1j2..gws-wiz.....0.0i71.IPXZzI1vg60. [Accessed: 04-Mar-2019].
- [26] N. E. Yang, J. W. Lee, and R. H. Park, "Depth Map Generation Using Local Depth Hypothesis for 2D-TO-3D Conversion," *Int. J. Comput. Graph. Animat.*, vol. 3, no. 1, pp. 1–15, Jan. 2013.
- [27] R. Phan, R. Rzeszutek, and D. Androutsos, "Semi-automatic 2D to 3D image conversion using scale-space Random Walks and a graph cuts based depth prior," in *2011 18th IEEE International Conference on Image Processing*, Brussels, Belgium, 2011, pp. 865–868.
- [28] A. Bouchemel, D. Abed, and A. Moussaoui, "Enhancement of Compressed Image Transmission in WMSNs Using Modified μ -Nonlinear Transformation," *IEEE Commun. Lett.*, vol. 22, no. 5, pp. 934–937, May 2018.
- [29] J. Mukherjee and S. K. Mitra, "Enhancement of Color Images by Scaling the DCT Coefficients," *IEEE Trans. Image Process.*, vol. 17, no. 10, pp. 1783–1794, Oct. 2008.
- [30] Y. Yang, Q. Liu, X. He, and Z. Liu, "Cross-View Multi-Lateral Filter for Compressed Multi-View Depth Video," *IEEE Trans. Image Process.*, vol. 28, no. 1, pp. 302–315, Jan. 2019.
- [31] H.-G. Jeon *et al.*, "Accurate depth map estimation from a lenslet light field camera," in *2015 IEEE Conference on Computer Vision and Pattern Recognition (CVPR)*, Boston, MA, USA, 2015, pp. 1547–1555.
- [32] I. U. Afridi, T. Bashir, H. A. Khattak, T. M. Khan, and M. Imran, "Degraded image enhancement by image dehazing and Directional Filter Banks using Depth Image based Rendering for future free-view 3D-TV," *PLOS ONE*, vol. 14, no. 5, p. e0217246, May 2019.
- [33] S. Zhuo and T. Sim, "Defocus map estimation from a single image," *Pattern Recognit.*, vol. 44, no. 9, pp. 1852–1858, Sep. 2011.